

Probing dynamical symmetries by bicircular high-order harmonic spectroscopy beyond the Born-Oppenheimer approximation

Shengjun Yue ^{1,2}, Simon Brennecke,² Hongchuan Du,^{1,*} and Manfred Lein ^{2,†}

¹*School of Nuclear Science and Technology, Lanzhou University, Lanzhou 730000, China*

²*Leibniz University Hannover, Institute of Theoretical Physics, Appelstraße 2, 30167 Hannover, Germany*



(Received 17 February 2020; accepted 5 May 2020; published 28 May 2020)

We explore the possibility of bicircular high-order harmonic spectroscopy to probe the laser-induced dynamics of molecules in a non-Born-Oppenheimer treatment. The numerical solutions of the time-dependent Schrödinger equation for aligned H₂ and its isotopologs in ω - 2ω bicircular fields show that the intensity ratio between D₂ and H₂ for harmonic orders $3q$ is lower than that for orders $3q \pm 1$ ($q \in \mathbb{N}$). Based on the strong-field approximation, we demonstrate that the interplay of vibrational wave-packet motion and dynamical-symmetry breaking leads to the different ratio. In general, the vibrational motion causes the ratio between isotopologs to increase with q for both harmonic orders $3q$ and $3q \pm 1$. On the other hand, the emission of orders $3q$ is possible only because of the alignment-induced breaking of the dynamical symmetry. The faster nuclear motion in H₂ enhances the symmetry breaking, resulting in the lower D₂/H₂ ratio for the orders $3q$. Therefore, the harmonic orders $3q$ give access to the attosecond probing of dynamical symmetries in molecules.

DOI: [10.1103/PhysRevA.101.053438](https://doi.org/10.1103/PhysRevA.101.053438)

I. INTRODUCTION

High-order harmonic generation (HHG) from atoms and molecules driven by strong laser fields has important applications in attosecond science [1–8]. The process of HHG can be qualitatively described by the classical three-step model [9,10] or its quantum-mechanical formulation, the Lewenstein model, also known as strong-field approximation (SFA) [11]. In the first step, an electron is removed through the potential barrier formed by the atomic or molecular potential and the laser field. In the second step, the electron is accelerated in the oscillating laser field. Finally, the electron may return to the parent ion and may recombine with the ion, emitting an extreme ultraviolet photon. Since these processes occur on the attosecond time scale and they create a mapping between electron trajectories and photon energies [12], HHG spectra are useful for probing the ultrafast dynamics of atoms and molecules [13,14].

The fundamental challenge in attosecond science is the probing of rapidly evolving processes in atoms and molecules. The present work is related to the following two important developments in this area. One is the investigation of the vibrational motion in molecules, including isotope effects [15–24]. It offers two important schemes to detect ultrafast processes inside molecules, since the laser-driven nuclear motion introduces amplitude modulation [15,16] and frequency modulation [22,24,25] in harmonic signals via the essential new degree of freedom, the internuclear distance. The other is the use of nontrivial forms of laser pulses, such as parallel two-color fields [26], orthogonal two-color fields [27–31],

and bicircular fields [32–34]. Bicircular high-order harmonic spectroscopy, especially, has received attention in theory and experiment owing to its sensitivity to electronic structure [35], chirality [36–38], and atomic and molecular symmetries [39–43].

Symmetry is the origin of selection rules in HHG [44–47]. Such selection rules are important in the study of molecular structure and dynamics [14,48]. A precise analysis involves the concept of “dynamical symmetry” [46], which means that the time-dependent Hamiltonian describing the target and external field is invariant under a transformation that combines a time translation and a spatial transformation such as inversion or rotation. The most widely known example is the generation of odd-order harmonics in HHG when linearly polarized laser pulses and inversion-symmetric targets such as atoms are used [44]. The breaking of inversion symmetry leads to the emission of additional even-order harmonics [44,49], which can be used as a tool to measure molecular wave-packet dynamics [49,50]. Recently, it has been demonstrated that HHG with bicircular fields provides a probe of dynamical symmetries in atoms and molecules [42]: For an ω - 2ω bicircular field, the harmonic orders $3q$ ($q \in \mathbb{N}$) are forbidden in threefold-symmetric systems (such as atoms plus the bicircular field). If the threefold symmetry is perturbed, the orders $3q$ become observable. In Ref. [42], this has been demonstrated by femtosecond pump-probe measurements. However, the interplay of dynamical symmetry in molecules and the vibrational motion on the attosecond time scale has not been addressed previously.

In this article, we investigate HHG from the hydrogen molecule and its isotopologs driven by ω - 2ω bicircular laser fields beyond the Born-Oppenheimer (BO) approximation. We observe that the intensity ratio between D₂ and H₂ for harmonic orders $3q \pm 1$ ($q \in \mathbb{N}$) is similar to the results obtained

*duhch@lzu.edu.cn

†lein@itp.uni-hannover.de

with linearly polarized laser fields [15]. Interestingly, the ratio between D_2 and H_2 for harmonic orders $3q$ is smaller than that for harmonic orders $3q \pm 1$. These results can be well interpreted by invoking two factors: the vibrational wave function of nuclear motion and the dynamical-symmetry breaking. This is clearly demonstrated through a SFA-type analysis for HHG in ω - 2ω bicircular fields. Hence, in bicircular fields, the intracycle nuclear motion can be reconstructed from the ratio between D_2 and H_2 for harmonic orders $3q \pm 1$ [15] and the ratio for harmonic orders $3q$ is sensitive to symmetry breaking. This is a potential tool to probe time-dependent dynamical symmetries inside molecules.

II. THEORETICAL MODEL

We describe the laser-driven correlated electronic and nuclear dynamics using a non-BO single-active electron model of H_2 . In this model, the electron moves in two-dimensional space with a Cartesian coordinate \mathbf{r} . The orientation θ of the molecule with respect to the field is held frozen, since the rotational motion can be neglected on the few-cycle time scale. The effective Hamiltonian for the interaction with a laser field $\mathbf{E}(t)$ takes the form (Hartree atomic units are used throughout)

$$H_{\text{eff}} = -\frac{\partial_{\mathbf{r}}^2}{2M_n} - \frac{\partial_{\mathbf{r}}^2}{2M_e} + V_{\text{eff}}(R, \mathbf{r}) + \mathbf{r} \cdot \mathbf{E}(t), \quad (1)$$

where $M_n = M_1 M_2 / (M_1 + M_2)$ and $M_e = (M_1 + M_2) / (M_1 + M_2 + 1)$ are the reduced masses of the nuclei and electron, respectively, with $M_{1,2}$ being the masses of the nuclei. R is the internuclear distance. The effective potential is chosen as [15]

$$V_{\text{eff}}(R, \mathbf{r}) = V_{\text{BO}}^+(R) - \sum_{j=1,2} \frac{Z(R, |\mathbf{r} - \mathbf{R}_j|)}{\sqrt{|\mathbf{r} - \mathbf{R}_j|^2 + 0.5}}, \quad (2)$$

where $V_{\text{BO}}^+(R)$ is the BO ground-state potential of H_2^+ created by the inactive electron. \mathbf{R}_j represent the positions of the two nuclei. Here, the effective nuclear charge $Z(R, r) = [1 + \exp(-r^2/\sigma^2(R))]/2$ is introduced to describe screening, i.e., $Z(R, r) \xrightarrow{r \rightarrow \infty} 1/2$ and $Z(R, r) \xrightarrow{r \rightarrow 0} 1$. The parameter $\sigma(R)$ is adjusted such that the lowest BO potential-energy curve of the Hamiltonian matches that of real H_2 . This model does not include electronic excitation of the molecular ion. From previous work [51] on HHG with linear polarization at parameters comparable to the present work, we judge that excitation of the ion plays a negligible role when HHG is dominated by short electron trajectories. Importantly, however, the model includes vibrational motion of the molecular ion. When the active electron is far from the core, the vibrational motion is governed by the BO potential V_{BO}^+ . This means that ionization initiates vibrational dynamics in the ion, including also a small but unimportant fraction of dissociation. The ω - 2ω bicircular field composed of two counter-rotating components with equal field strengths [52,53] reads

$$\mathbf{E}(t) = E_0 f(t) \left[\begin{pmatrix} \cos(\omega t) \\ \sin(\omega t) \end{pmatrix} + \begin{pmatrix} \cos(2\omega t) \\ -\sin(2\omega t) \end{pmatrix} \right]. \quad (3)$$

E_0 is the electric-field amplitude of each component of the bicircular field and ω is the frequency of the fundamental laser field. The bicircular field has a trapezoidal envelope $f(t)$ with

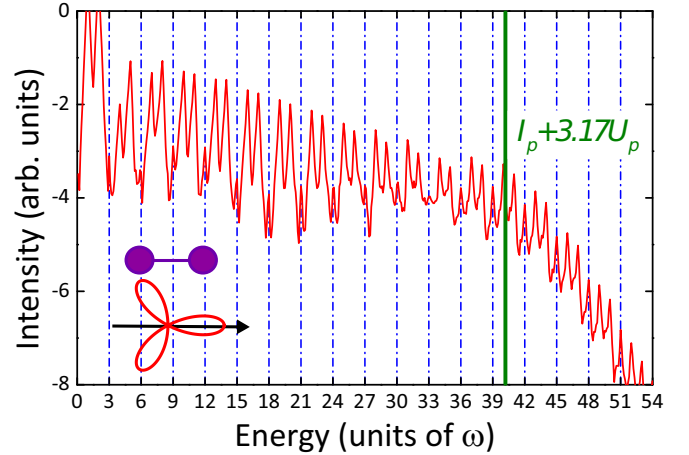


FIG. 1. The harmonic spectra for H_2 in a 912/456 nm pulse with total intensity $3.51 \times 10^{14} \text{ W/cm}^2$. The sketch in the lower left part illustrates the direction of the molecular axis relative to the applied electric field.

a total duration of eight optical cycles including two-cycle linear ramps.

The time-dependent Schrödinger equation (TDSE) is numerically solved by the Crank-Nicolson method [54,55] with a time step of 0.1 a.u. The grid ranges from -170 to 170 a.u. for the electron and from 0.5 to 20 a.u. for the internuclear distance with the grid spacings $\Delta x = \Delta y = \Delta R = 0.1$ a.u. Absorbing boundaries with a $\cos^{1/8}$ -shaped mask function are employed to avoid reflections of the wave function for all coordinates. The ground state of neutral molecules is prepared by imaginary-time propagation [56]. The dipole acceleration can be obtained through the Ehrenfest theorem [57]:

$$\mathbf{a}(t) = \frac{1}{M_e} \langle \psi(t) | \partial_{\mathbf{r}}(V_{\text{eff}} + \mathbf{r} \cdot \mathbf{E}(t)) | \psi(t) \rangle. \quad (4)$$

The total bicircular high-order harmonic spectrum can be calculated from the Fourier transform of the dipole acceleration,

$$P_{\text{tot}}(\Omega) = \sum_{n=x,y} \left| \frac{1}{\sqrt{2\pi}} \int_{-\infty}^{+\infty} a_n(t) e^{i\Omega t} dt \right|^2, \quad (5)$$

with the harmonic frequency Ω . $a_n(t)$ represent the x and y components of the dipole acceleration. To evaluate the harmonic intensity at harmonic order N ($N \in \mathbb{N}$), we integrate the signal over one harmonic peak at $\Omega = N\omega$.

III. RESULTS AND DISCUSSIONS

A. TDSE results

Figure 1 shows one representative HHG spectrum for aligned H_2 in a 912/456 nm bicircular pulse with total intensity $3.51 \times 10^{14} \text{ W/cm}^2$. The molecular axis is aligned along the x axis. The combination of generating medium and laser field possesses C_1 symmetry using the notation of Ref. [47]. Therefore, all integer harmonic orders are generated in Fig. 1, including orders $3q$ which are symmetry forbidden in atoms. Moreover, the harmonic spectrum exhibits a slow decrease with energy and a cutoff not far from the

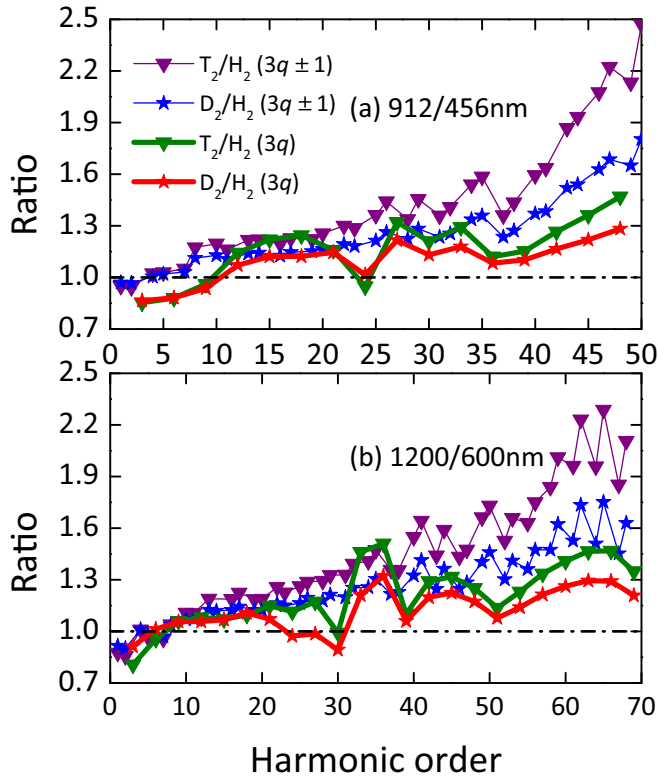


FIG. 2. Ratios of harmonic intensities in different isotopologs (aligned along the x axis) as a function of harmonic order for (a) 912/456 nm and (b) 1200/600 nm. Results are shown for harmonic orders $3q \pm 1$ and $3q$ as indicated. The field amplitudes are (a) $E_0 = 0.05$ a.u. and (b) $E_0 = 0.04$ a.u.

energy $I_p + 3.17U_p$. Here, I_p is the vertical ionization potential and $U_p = (2E_0)^2/4\bar{\omega}^2$ is an effective ponderomotive energy, where $2E_0$ is the sum of the electric field amplitudes of the two components of the bicircular field and $\bar{\omega} = (\omega + 2\omega)/2$ is the average frequency of the bicircular field. By transforming to a rotating frame, the bicircular field becomes linearly polarized with frequency $\bar{\omega}$, which explains the success of the simple expression for the cutoff [58–60].

We compare the harmonic spectra of H_2 , D_2 , and T_2 , aligned parallel to the x axis, driven by the ω - 2ω bicircular laser field. The simulations are carried out at different fundamental wavelengths. We use 912/456 nm pulses (with amplitude $E_0 = 0.05$ a.u., total intensity 3.51×10^{14} W/cm²) in Fig. 2(a) and 1200/600 nm pulses (with amplitude $E_0 = 0.04$ a.u., total intensity 2.25×10^{14} W/cm²) in Fig. 2(b). We find that in both cases the ratios between different isotopologs for harmonic orders $3q \pm 1$ are consistent with the results in Refs. [15,16], where linearly polarized laser pulses were used. Usually, heavier isotopologs generate stronger harmonics and the ratio between the different isotopologs increases with harmonic order. This is explained by the slower nuclear motion in the heavier isotopologs together with the fact that higher harmonic orders imply longer time intervals for the vibrational wave-packet evolution [15,16,23] (see below for further details). This concept is applicable to any molecular orientation [61]. For D_2 ($3q \pm 1$) over H_2 ($3q \pm 1$), the ratio reaches about 1.7 beyond the cutoff. Interestingly, however,

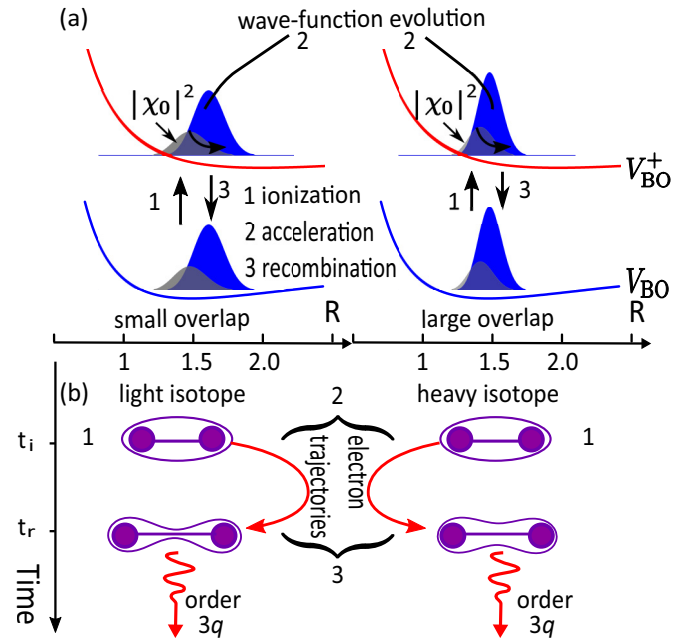


FIG. 3. Illustration of the mechanism of molecular HHG for a light isotopolog on the left and a heavy isotopolog on the right. (a) Vibrational wave-packet dynamics (quantitative results for the initial and final wave packets in H_2 and D_2 as they appear in the SFA-based theory for laser parameters as in Fig. 1 and harmonic order 52). Here, the initial ground state is normalized. However, the norm of the wave packet is not conserved due to the excursion of the electron in complex time. (b) Increase of symmetry breaking by bond stretching (qualitative).

the ratios at harmonic orders $3q$ are smaller than those at harmonic orders $3q \pm 1$.

By considering two important factors in HHG, namely, the vibrational wave-packet dynamics and the dynamical symmetry, the above TDSE results can be interpreted. Illustrations of these two aspects are shown in Fig. 3. In Fig. 3(a), a wave packet is launched into the lowest BO potential V_{BO}^+ of the ion when the active electron is removed from the initial state of the neutral molecule. The nuclear wave packet undergoes a time evolution during the continuum travel of the active electron. The overlap between the real initial wave function χ_0 and the evolved wave function at the recombination time t_r influences decisively the strength of harmonic emission. Higher overlap leads to stronger harmonic generation. Figure 3(a) shows the quantitative results for the initial and evolved vibrational wave packets in H_2 and D_2 in the case of harmonic order 52 for the parameters of Fig. 1. Here, we use the complex electron excursion time that arises in the SFA-based theory (see next section) as the time span for vibrational evolution, which leads to the nonconserved norm of the wave packet. The isotope effect is visible in the plot: the wave-function overlap is larger in the case of the heavier isotopolog due to the slower nuclear motion. Figure 3(b) illustrates the dynamical-symmetry breaking. The ω - 2ω bicircular electric field with a threefold symmetry describes a Lissajous figure, resembling a clover leaf (see Fig. 1). On the interaction of such a pulse with the aligned H_2 , the otherwise symmetry-forbidden harmonic orders at $3q$ are emitted because the threefold symmetry

is broken by the alignment [42,47]. Reference [42] showed that the symmetry breaking does not significantly affect the harmonic orders $3q \pm 1$ in their setup. In our case, while the symmetry breaking is always present, it is more pronounced for the lighter isotopolog because the faster expansion of the system after the ionization step causes a stronger deviation of the electron wave function from spherical symmetry. Figure 3(b) shows a qualitative sketch of this effect.

Therefore, the ratios found in the TDSE results can be understood as follows. The small nuclear mass of H_2 means a fast separation of the nuclei. This causes a more rapid decrease of the vibrational overlap compared to D_2/T_2 , weakening both harmonic orders $3q$ and $3q \pm 1$ [15,16]. However, faster nuclear motion also results in a higher degree of symmetry breaking. This implies more intense signals for harmonic orders $3q$ but only a slight variation in harmonic orders $3q \pm 1$. As a result, the ratio for orders $3q \pm 1$ is similar to the results in linear polarization, whereas the ratio for orders $3q$ is lower.

B. SFA model with vibrational motion

We give a quantitative modeling on the basis of the above explanation using SFA [62] for vibrating molecules in bicircular driving fields. Previous theory [15,61] has already extended the Lewenstein model [11] to include the vibrational motion in diatomic molecules. In the extended SFA, the dependence of HHG on the electronic structure of the system is captured by the recombination transition matrix element $\mathbf{d}_{\text{rec}}(t_i, t_r, \mathbf{R})$, which is a function of the internuclear vector \mathbf{R} . This implies an orientation dependence of \mathbf{d}_{rec} , i.e., the spherical symmetry is broken. The degree of symmetry breaking depends on the internuclear distance R , which, in turn, is determined by the nuclear motion. Effectively, the harmonic vectorial amplitude is proportional to the following integral over R [61],

$$\begin{aligned} C(t_i, t_r) &= e^{-i(S(t_i, t_r) - \Omega t_r)} \\ &\times \int_0^\infty dR \mathbf{d}_{\text{rec}}(t_i, t_r, \mathbf{R}) \chi_0(R) U_R^+(t_r - t_i) \chi_0(R), \end{aligned} \quad (6)$$

with the semiclassical action $S(t_i, t_r) = \frac{1}{2} \int_{t_i}^{t_r} dt' [\mathbf{k}(t_i, t_r) + \mathbf{A}(t')]^2 + I_p(t_r - t_i)$ and the time-evolution operator for nuclear motion, U_R^+ . This time-evolution operator propagates the vibrational wave function according to the one-dimensional TDSE $i\partial_t \chi(R, t) = [-\partial_R^2/(2M_n) + \tilde{V}_{\text{BO}}^+(R)] \chi(R, t)$ with $\tilde{V}_{\text{BO}}^+(R) = V_{\text{BO}}^+(R) - V_{\text{BO}}^+(\langle \chi_0 | R | \chi_0 \rangle)$. Here, a constant has been added to the BO potential of H_2^+ to be consistent with the use of the vertical ionization potential I_p rather than the absolute value of the H_2 ground-state energy in the SFA action. The effect of the laser field on the vibrational dynamics of H_2^+ is neglected. This is consistent with the single-active-electron approximation used in the TDSE model, which implies that, after removal of the active electron, the ion remains in the electronic ground state and it is not affected by the laser field. The times of ionization, t_i , and recombination, t_r , are calculated by solving the corresponding saddle-point equations for the bicircular

field:

$$\frac{[\mathbf{k}(t_i, t_r) + \mathbf{A}(t_i)]^2}{2} = -I_p, \quad (7)$$

$$\frac{[\mathbf{k}(t_i, t_r) + \mathbf{A}(t_r)]^2}{2} = \Omega - I_p. \quad (8)$$

Here, we define the vertical ionization potential as $I_p = V_{\text{BO}}^+(R_0) - \varepsilon_0$, where ε_0 is the ground-state energy of the neutral molecule and R_0 is its equilibrium distance. The saddle-point momentum is $\mathbf{k}(t_i, t_r) = -\int_{t_i}^{t_r} dt' \mathbf{A}(t')/(t_r - t_i)$. In the linear combination of atomic orbitals approximation [63], and using the velocity form, the recombination matrix element is $\mathbf{d}_{\text{rec}}(t_i, t_r, \mathbf{R}) \propto \mathbf{v}(t_i, t_r) \cos(\mathbf{v}(t_i, t_r) \cdot \mathbf{R}/2)$. Here, the velocity of the electron at the return time t_r is $\mathbf{v}(t_i, t_r) = \mathbf{k}(t_i, t_r) + \mathbf{A}(t_r)$ with the vector potential $\mathbf{A}(t) = -\int^t dt' \mathbf{E}(t')$.

In a bicircular driving field with threefold dynamical symmetry [64], we have

$$\mathbf{E}\left(t + \frac{T}{3}\right) = D_{\frac{2\pi}{3}} \mathbf{E}(t) \quad (9)$$

with the period T of the fundamental field and the rotation matrix $D_{\frac{2\pi}{3}}$ representing the rotation by an angle of $\frac{2\pi}{3}$ around the z axis. The vector potential $\mathbf{A}(t)$ fulfills the same symmetry. If t_i and t_r are saddle-point times, i.e., solutions of Eqs. (7) and (8), then also $t_i + \frac{T}{3}$ and $t_r + \frac{T}{3}$ are solutions. Based on the symmetry in Eq. (9), we find

$$\mathbf{k}\left(t_i + \frac{T}{3}, t_r + \frac{T}{3}\right) = D_{\frac{2\pi}{3}} \mathbf{k}(t_i, t_r), \quad (10)$$

$$\mathbf{v}\left(t_i + \frac{T}{3}, t_r + \frac{T}{3}\right) = D_{\frac{2\pi}{3}} \mathbf{v}(t_i, t_r), \quad (11)$$

$$S\left(t_i + \frac{T}{3}, t_r + \frac{T}{3}\right) = S(t_i, t_r). \quad (12)$$

The time-shifted recombination transition matrix element satisfies

$$\mathbf{d}_{\text{rec}}\left(t_i + \frac{T}{3}, t_r + \frac{T}{3}, \mathbf{R}\right) = D_{\frac{2\pi}{3}} \mathbf{d}_{\text{rec}}\left(t_i, t_r, D_{\frac{2\pi}{3}}^{-1} \mathbf{R}\right). \quad (13)$$

$D_{\frac{2\pi}{3}}^{-1}$ denotes a rotation by an angle of $\frac{2\pi}{3}$ in the opposite direction of $D_{\frac{2\pi}{3}}$. The summation of harmonic amplitudes from the three short trajectories in one optical cycle of the fundamental field, projected on the polarization vectors $\mathbf{e}_\pm = (\mathbf{e}_x \pm i\mathbf{e}_y)/\sqrt{2}$ for left and right circular polarization, can thus be written as

$$\begin{aligned} C^\pm(\Omega) &= e^{-i\tilde{S}} \int_0^\infty dR \sum_{j=0}^2 e^{i\frac{2\pi j}{3}(\frac{\Omega}{\omega} \mp 1)} \mathbf{e}_\pm^* \cdot \mathbf{v}(t_i, t_r) \\ &\times \cos\left(\frac{\mathbf{v}(t_i, t_r) \cdot D_{\frac{2\pi j}{3}}^{-1} \mathbf{R}}{2}\right) \chi_0(R) U_R^+(\tau) \chi_0(R) \end{aligned} \quad (14)$$

with $\tilde{S} = S(t_i, t_r) - \Omega t_r$ and excursion time $\tau = \tau(\Omega) = t_r(\Omega) - t_i(\Omega)$. In Eq. (14), if the recombination matrix element is independent of the direction of \mathbf{R} , the frequencies $\Omega = 3\omega q$ are symmetry forbidden due to destructive

interference of the contributions from three short trajectories, i.e., $C^\pm(3\omega q) = 0$.

The total intensity ratio between D_2 and H_2 is approximated as

$$R_a(\Omega) = \frac{|C_D^-(\Omega)|^2 + |C_D^+(\Omega)|^2}{|C_H^-(\Omega)|^2 + |C_H^+(\Omega)|^2}. \quad (15)$$

In the SFA calculations, we use the complex times t_i and t_r of the short trajectory. Note that, as discussed in Ref. [62], an electron has to start with an appropriate initial transverse velocity in order to return to the parent ion on a classical trajectory. Since for the long trajectories much larger initial velocities are needed compared to the short trajectories, and because larger velocities imply smaller probabilities, these contributions are effectively suppressed. Thus the short trajectories make the dominant contribution to HHG, which is also confirmed in our numerical results. We use the Gabor time-frequency analysis [65,66] to isolate this trajectory in the TDSE results. The total harmonic intensity is the coherent sum over the relevant time windows at times t_j ($j \in \mathbb{N} | 1 \leq j \leq 12$) that contribute to the short trajectories in the flat-top part of the trapezoidal pulse,

$$I_G(\Omega) = I_{G_x}(\Omega) + I_{G_y}(\Omega) = \sum_{n=x,y} \left| \sum_{j=1}^{12} \bar{G}_n(\Omega, t_j) \right|^2, \quad (16)$$

with $\bar{G}_n(\Omega, t_j) = \int_{t_j}^{t_j+\Delta t} dt G_n(\Omega, t)$ and the Gabor transform

$$G_n(\Omega, t) = \int dt' a_n(t') e^{-(t'-t)^2/(2\zeta^2)} e^{i\Omega t'}. \quad (17)$$

We choose $\zeta = 1/(3\omega)$.

Figure 4 shows the intensity ratios between D_2 and H_2 for various orientations obtained by SFA and TDSE calculations. The laser parameters are the same as in Fig. 2(a). The harmonic orders $3q - 1$ are excluded from Fig. 4, since they show the same trend as harmonic orders $3q + 1$. In general, the TDSE ratios of both harmonic orders $3q + 1$ and $3q$ are slightly reduced due to the elimination of long trajectories when compared to Fig. 2(a). This happens because the D_2/H_2 ratio for the long trajectory is higher than that for the short trajectory, which has been reported and explained previously [23,51]. The reason is essentially that longer excursion times allow for longer vibrational motion and therefore to an increased difference between HHG in D_2 and H_2 . Also, the trajectory selection leads to smoother curves. We find good agreement between SFA and TDSE results. In particular, the difference between the ratios for $3q + 1$ and $3q$ is evident in both types of calculations. Similar results are obtained for the case of 1200/600 nm. These results are only weakly dependent on the molecular orientation as shown in Fig. 4.

Our results are significantly influenced by both vibrational dynamics and dynamical symmetry breaking. This implies that both phenomena occur on a similar time scale, namely, the attosecond time scale of electron trajectories.

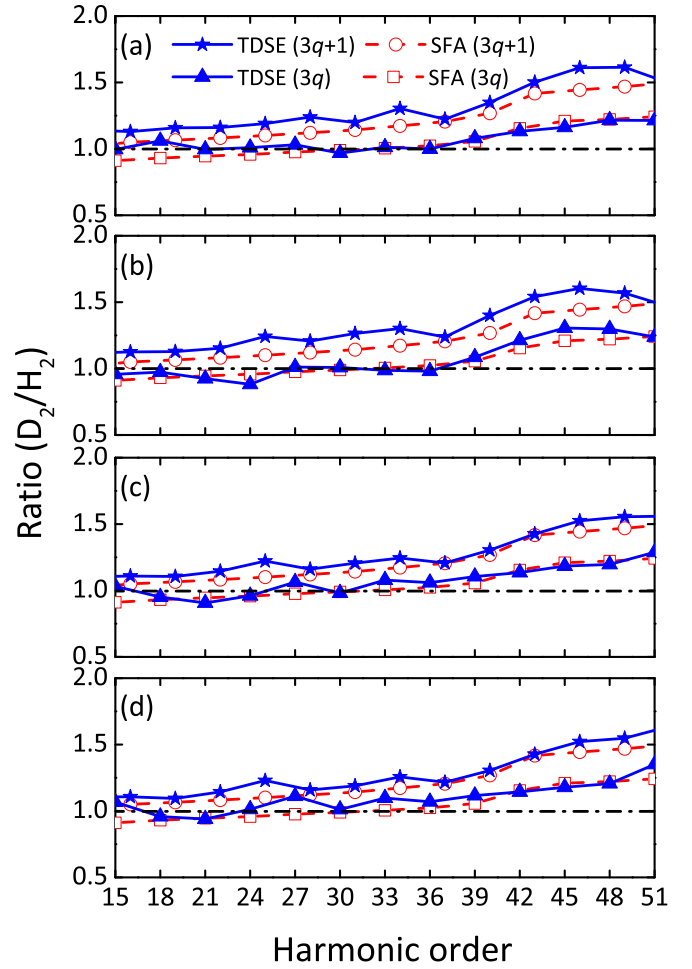


FIG. 4. Harmonic intensity ratio between D_2 and H_2 in a 912/456 nm bicircular pulse with 3.51×10^{14} W/cm² total intensity as a function of harmonic order. Solid blue lines are TDSE results for $3q + 1$ (stars) and $3q$ (triangles). Here, only short trajectories are retained in the TDSE analysis. The corresponding SFA results $R_a(\Omega)$ are displayed as circles ($3q + 1$) and squares ($3q$) connected by dashed red lines. The orientation of the molecules with respect to the x axis is (a) $\theta = 0^\circ$, (b) $\theta = 50^\circ$, (c) $\theta = 80^\circ$, and (d) $\theta = 90^\circ$.

IV. CONCLUSIONS

In summary, we have studied HHG in a non-BO model of aligned H_2 , D_2 , and T_2 interacting with ω - 2ω bicircular fields. The TDSE simulations show that the harmonic intensity ratios D_2/H_2 and T_2/H_2 for harmonic orders $3q \pm 1$ and $3q$ differ. SFA results agree well with the TDSE results. Two main reasons, the vibrational wave-packet motion and the dynamical symmetry, give rise to the different ratios. On the one hand, the vibrational motion weakens harmonics of all allowed harmonic orders ($3q \pm 1$ and $3q$) in lighter isotopologs due to the faster nuclear motion, which is familiar from previous theory and experiment [15,16]. On the other hand, generation of harmonic orders $3q$ is allowed only when the threefold dynamical symmetry is violated. In the lighter isotopologs, the degree of symmetry breaking induced by the faster vibrational motion is higher than in the heavier isotopologs so that this effect prefers the lighter species, which finally results in the lowered harmonic intensity ratio for the orders

3*q*. The dependence of the ratio on the electron excursion time reflects the attosecond-scale dynamics of the symmetry breaking. Observation of these effects requires HHG from an aligned sample of molecules. Although this is difficult to achieve with H₂ molecules, we note that partial laser-induced alignment was found in previous experiments on H₂ and D₂ when sufficiently long linearly polarized femtosecond pulses were used [17].

ACKNOWLEDGMENTS

We gratefully acknowledge valuable discussions with Xiaosong Zhu. This work was supported by the China Scholarship Council (CSC) and the National Natural Science Foundation of China (Grant No. 11874030). We thank the Deutsche Forschungsgemeinschaft for support within the Priority Programme Quantum Dynamics in Tailored Intense Fields (QUTIF).

-
- [1] Z. Chang, A. Rundquist, H. Wang, M. M. Murnane, and H. C. Kapteyn, Generation of Coherent Soft X Rays at 2.7 nm Using High Harmonics, *Phys. Rev. Lett.* **79**, 2967 (1997).
- [2] P. M. Paul, E. Toma, P. Breger, G. Mullot, F. Augé, P. Balcou, H. Muller, and P. Agostini, Observation of a train of attosecond pulses from high harmonic generation, *Science* **292**, 1689 (2001).
- [3] R. Kienberger, E. Goulielmakis, M. Uiberacker, A. Baltuska, V. Yakovlev, F. Bammer, A. Scrinzi, T. Westerwalbesloh, U. Kleineberg, U. Heinzmann, M. Drescher, and F. Krausz, Atomic transient recorder, *Nature (London)* **427**, 817 (2004).
- [4] J. Itatani, J. Jérôme, D. Zeidler, H. Niikura, H. Pépin, J.-C. Kieffer, P. B. Corkum, and D. M. Villeneuve, Tomographic imaging of molecular orbitals, *Nature (London)* **432**, 867 (2004).
- [5] T. Kanai, S. Minemoto, and H. Sakai, Quantum interference during high-order harmonic generation from aligned molecules, *Nature (London)* **435**, 470 (2005).
- [6] W. Li, X. Zhou, R. Lock, S. Patchkovskii, A. Stolow, H. C. Kapteyn, and M. M. Murnane, Time-resolved dynamics in N₂O₄ probed using high harmonic generation, *Science* **322**, 1207 (2008).
- [7] T. Morishita, A. T. Le, Z. Chen, and C. D. Lin, Accurate Retrieval of Structural Information from Laser-Induced Photoelectron and High-Order Harmonic Spectra by Few-Cycle Laser Pulses, *Phys. Rev. Lett.* **100**, 013903 (2008).
- [8] C. Vozzi, M. Negro, F. Calegari, G. Sansone, M. Nisoli, S. De Silvestri, and S. Stagira, Generalized molecular orbital tomography, *Nat. Phys.* **7**, 822 (2011).
- [9] K. C. Kulander, K. J. Schafer, and J. L. Krause, Dynamics of short-pulse excitation, ionization and harmonic conversion, in *Super-Intense Laser-Atom Physics*, edited by B. Pireaux, A. L'Huillier, and K. Rzażewski, NATO ASI, Series B: Physics (Springer, Boston, 1993), Vol. 316.
- [10] P. B. Corkum, Plasma Perspective on Strong Field Multiphoton Ionization, *Phys. Rev. Lett.* **71**, 1994 (1993).
- [11] M. Lewenstein, P. Balcou, M. Y. Ivanov, A. L'Huillier, and P. B. Corkum, Theory of high-harmonic generation by low-frequency laser fields, *Phys. Rev. A* **49**, 2117 (1994).
- [12] Y. Mairesse, A. De Bohan, L. J. Frasinski, H. Merdji, L. C. Dinu, P. Monchicourt, P. Breger, M. Kovacčev, R. Taïeb, B. Carré, H. G. Muller, P. Agostini, and P. Salères, Attosecond synchronization of high-harmonic soft X-rays, *Science* **302**, 1540 (2003).
- [13] O. Smirnova, Y. Mairesse, S. Patchkovskii, N. Dudovich, D. Villeneuve, P. Corkum, and M. Y. Ivanov, High harmonic interferometry of multi-electron dynamics in molecules, *Nature (London)* **460**, 972 (2009).
- [14] P. M. Kraus, B. Migolet, D. Baykusheva, A. Rupenyany, L. Horný, E. F. Penka, G. Grassi, O. I. Tolstikhin, J. Schneider, F. Jensen, L. B. Madsen, A. D. Bandrauk, F. Remacle, and H. J. Wörner, Measurement and laser control of attosecond charge migration in ionized iodoacetylene, *Science* **350**, 790 (2015).
- [15] M. Lein, Attosecond Probing of Vibrational Dynamics with High-Harmonic Generation, *Phys. Rev. Lett.* **94**, 053004 (2005).
- [16] S. Baker, J. S. Robinson, C. Haworth, H. Teng, R. Smith, C. C. Chirilă, M. Lein, J. Tisch, and J. P. Marangos, Probing proton dynamics in molecules on an attosecond time scale, *Science* **312**, 424 (2006).
- [17] S. Baker, J. S. Robinson, M. Lein, C. C. Chirilă, R. Torres, H. C. Bandulet, D. Comtois, J. C. Kieffer, D. M. Villeneuve, J. W. G. Tisch, and J. P. Marangos, Dynamic Two-Center Interference in High-Order Harmonic Generation from Molecules with Attosecond Nuclear Motion, *Phys. Rev. Lett.* **101**, 053901 (2008).
- [18] M. Falge, V. Engel, and M. Lein, Vibrational-state and isotope dependence of high-order harmonic generation in water molecules, *Phys. Rev. A* **81**, 023412 (2010).
- [19] J. P. Farrell, S. Petretti, J. Förster, B. K. McFarland, L. S. Spector, Y. V. Vanne, P. Decleva, P. H. Bucksbaum, A. Saenz, and M. Gühr, Strong Field Ionization to Multiple Electronic States in Water, *Phys. Rev. Lett.* **107**, 083001 (2011).
- [20] P. M. Kraus and H. J. Wörner, Attosecond nuclear dynamics in the ammonia cation: Relation between high-harmonic and photoelectron spectroscopies, *ChemPhysChem* **14**, 1445 (2013).
- [21] J. Förster and A. Saenz, Theoretical study of the inversion motion of the ammonia cation with subfemtosecond resolution for high-harmonic spectroscopy, *ChemPhysChem* **14**, 1438 (2013).
- [22] X.-B. Bian and A. D. Bandrauk, Probing Nuclear Motion by Frequency Modulation of Molecular High-Order Harmonic Generation, *Phys. Rev. Lett.* **113**, 193901 (2014).
- [23] P. Lan, M. Ruhmann, L. He, C. Zhai, F. Wang, X. Zhu, Q. Zhang, Y. Zhou, M. Li, M. Lein, and P. Lu, Attosecond Probing of Nuclear Dynamics with Trajectory-Resolved High-Harmonic Spectroscopy, *Phys. Rev. Lett.* **119**, 033201 (2017).
- [24] L. He, Q. Zhang, P. Lan, W. Cao, X. Zhu, C. Zhai, F. Wang, W. Shi, M. Li, X.-B. Bian, P. Lu, and A. D. Bandrauk, Monitoring ultrafast vibrational dynamics of isotopic molecules with frequency modulation of high-order harmonics, *Nat. Commun.* **9**, 1108 (2018).
- [25] S. Yue, S. Fu, J. Li, X. Zhang, Y. Feng, B. Hu, and H. Du, A redshift mechanism of high-order harmonics: Change of ionization energy, *J. Chem. Phys.* **148**, 234304 (2018).
- [26] N. Dudovich, O. Smirnova, J. Levesque, Y. Mairesse, M. Y. Ivanov, D. Villeneuve, and P. B. Corkum, Measuring and

- controlling the birth of attosecond XUV pulses, *Nat. Phys.* **2**, 781 (2006).
- [27] H. Niikura, N. Dudovich, D. M. Villeneuve, and P. B. Corkum, Mapping Molecular Orbital Symmetry on High-Order Harmonic Generation Spectrum using Two-Color Laser Fields, *Phys. Rev. Lett.* **105**, 053003 (2010).
- [28] L. Brugnera, D. J. Hoffmann, T. Siegel, F. Frank, A. Zaïr, J. W. G. Tisch, and J. P. Marangos, Trajectory Selection in High Harmonic Generation by Controlling the Phase between Orthogonal Two-Color Fields, *Phys. Rev. Lett.* **107**, 153902 (2011).
- [29] D. Shafir, H. Soifer, B. D. Bruner, M. Dagan, Y. Mairesse, S. Patchkovskii, M. Y. Ivanov, O. Smirnova, and N. Dudovich, Resolving the time when an electron exits a tunnelling barrier, *Nature (London)* **485**, 343 (2012).
- [30] J. Zhao and M. Lein, Determination of Ionization and Tunneling Times in High-Order Harmonic Generation, *Phys. Rev. Lett.* **111**, 043901 (2013).
- [31] D. Faccialà, S. Pabst, B. D. Bruner, A. G. Ciriolo, S. De Silvestri, M. Devetta, M. Negro, H. Soifer, S. Stagira, N. Dudovich, and C. Vozzi, Probe of Multielectron Dynamics in Xenon by Caustics in High-Order Harmonic Generation, *Phys. Rev. Lett.* **117**, 093902 (2016).
- [32] O. Kfir, P. Grychtol, E. Turgut, R. Knut, D. Zusin, D. Popmintchev, T. Popmintchev, H. Nembach, J. M. Shaw, A. Fleischer, H. Kapteyn, M. Murnane, and O. Cohen, Generation of bright phase-matched circularly-polarized extreme ultraviolet high harmonics, *Nat. Photonics* **9**, 99 (2015).
- [33] L. Medišauskas, J. Wragg, H. van der Hart, and M. Y. Ivanov, Generating Isolated Elliptically Polarized Attosecond Pulses Using Bichromatic Counterrotating Circularly Polarized Laser Fields, *Phys. Rev. Lett.* **115**, 153001 (2015).
- [34] T. Fan, P. Grychtol, R. Knut, C. Hernández-García, D. D. Hickstein, D. Zusin, C. Gentry, P. F. J. Dollar, C. A. Mancuso, C. W. Hogle, O. Kfir, D. Legut, K. Carva, J. L. Ellis, K. M. Dorney, C. Chen, O. G. Shpyrko, E. E. Fullerton, O. Cohen, P. M. Oppeneer, D. B. Milošević, A. Becker, A. A. Jaroń-Becker, T. Popmintchev, M. M. Murnane, and H. C. Kapteyn, Bright circularly polarized soft X-ray high harmonics for X-ray magnetic circular dichroism, *Proc. Natl. Acad. Sci. USA* **112**, 14206 (2015).
- [35] D. Baykusheva, S. Brennecke, M. Lein, and H. J. Wörner, Signatures of Electronic Structure in Bicircular High-Harmonic Spectroscopy, *Phys. Rev. Lett.* **119**, 203201 (2017).
- [36] O. Smirnova, Y. Mairesse, and S. Patchkovskii, Opportunities for chiral discrimination using high harmonic generation in tailored laser fields, *J. Phys. B* **48**, 234005 (2015).
- [37] D. Baykusheva and H. J. Wörner, Chiral Discrimination through Bielliptical High-Harmonic Spectroscopy, *Phys. Rev. X* **8**, 031060 (2018).
- [38] Y. Harada, E. Haraguchi, K. Kaneshima, and T. Sekikawa, Circular dichroism in high-order harmonic generation from chiral molecules, *Phys. Rev. A* **98**, 021401(R) (2018).
- [39] D. M. Reich and L. B. Madsen, Illuminating Molecular Symmetries with Bicircular High-Order-Harmonic Generation, *Phys. Rev. Lett.* **117**, 133902 (2016).
- [40] S. Odžak, E. Hasović, and D. B. Milošević, High-order harmonic generation in polyatomic molecules induced by a bicircular laser field, *Phys. Rev. A* **94**, 033419 (2016).
- [41] A. D. Bandrauk, F. Mauger, and K.-J. Yuan, Circularly polarized harmonic generation by intense bicircular laser pulses: Electron recollision dynamics and frequency dependent helicity, *J. Phys. B* **49**, 23LT01 (2016).
- [42] D. Baykusheva, M. S. Ahsan, N. Lin, and H. J. Wörner, Bicircular High-Harmonic Spectroscopy Reveals Dynamical Symmetries of Atoms and Molecules, *Phys. Rev. Lett.* **116**, 123001 (2016).
- [43] E. Hasović, S. Odžak, W. Becker, and D. B. Milošević, High-order harmonic generation in non-planar molecules driven by a bicircular field, *Mol. Phys.* **115**, 1750 (2017).
- [44] N. Ben-Tal, N. Moiseyev, and A. Beswick, The effect of Hamiltonian symmetry on generation of odd and even harmonics, *J. Phys. B* **26**, 3017 (1993).
- [45] S. Long, W. Becker, and J. K. McIver, Model calculations of polarization-dependent two-color high-harmonic generation, *Phys. Rev. A* **52**, 2262 (1995).
- [46] O. E. Alon, V. Averbukh, and N. Moiseyev, Selection Rules for the High Harmonic Generation Spectra, *Phys. Rev. Lett.* **80**, 3743 (1998).
- [47] X. Liu, X. Zhu, L. Li, Y. Li, Q. Zhang, P. Lan, and P. Lu, Selection rules of high-order-harmonic generation: Symmetries of molecules and laser fields, *Phys. Rev. A* **94**, 033410 (2016).
- [48] P. M. Kraus, D. Baykusheva, and H. J. Wörner, Two-Pulse Field-Free Orientation Reveals Anisotropy of Molecular Shape Resonance, *Phys. Rev. Lett.* **113**, 023001 (2014).
- [49] P. M. Kraus, A. Rupenyau, and H. J. Wörner, High-Harmonic Spectroscopy of Oriented OCS Molecules: Emission of Even and Odd Harmonics, *Phys. Rev. Lett.* **109**, 233903 (2012).
- [50] E. Frumker, C. T. Hebeisen, N. Kajumba, J. B. Bertrand, H. J. Wörner, M. Spanner, D. M. Villeneuve, A. Naumov, and P. B. Corkum, Oriented Rotational Wave-Packet Dynamics Studies via High Harmonic Generation, *Phys. Rev. Lett.* **109**, 113901 (2012).
- [51] C. C. Chirilă and M. Lein, Effect of dressing on high-order harmonic generation in vibrating H₂ molecules, *Phys. Rev. A* **77**, 043403 (2008).
- [52] H. Eichmann, A. Egbert, S. Nolte, C. Momma, B. Wellegehausen, W. Becker, S. Long, and J. K. McIver, Polarization-dependent high-order two-color mixing, *Phys. Rev. A* **51**, R3414 (1995).
- [53] D. B. Milošević and W. Becker, Attosecond pulse trains with unusual nonlinear polarization, *Phys. Rev. A* **62**, 011403(R) (2000).
- [54] M. Nurhuda and F. H. M. Faisal, Numerical solution of time-dependent Schrödinger equation for multiphoton processes: A matrix iterative method, *Phys. Rev. A* **60**, 3125 (1999).
- [55] J. Crank and P. Nicolson, A practical method for numerical evaluation of solutions of partial differential equations of the heat-conduction type, *Proc. Cambridge Philos. Soc.* **43**, 50 (1947).
- [56] M. Protopapas, C. H. Keitel, and P. L. Knight, Atomic physics with super-high intensity lasers, *Rep. Prog. Phys.* **60**, 389 (1997).
- [57] P. Ehrenfest, Bemerkung über die angenäherte Gültigkeit der klassischen Mechanik innerhalb der Quantenmechanik, *Z. Phys.* **45**, 455 (1927).
- [58] D. M. Reich and L. B. Madsen, Rotating-frame perspective on high-order-harmonic generation of circularly polarized light, *Phys. Rev. A* **93**, 043411 (2016).

- [59] K. J. Yuan and A. D. Bandrauk, Above-threshold ionization in molecules by intense multiple-frequency circularly polarized laser pulses, *Phys. Rev. A* **98**, 023413 (2018).
- [60] M.-Z. Li, Y. Xu, G.-R. Jia, and X.-B. Bian, Controlling polarization of high-order harmonic generation by molecular alignment in a bicircular laser field, *Phys. Rev. A* **100**, 033410 (2019).
- [61] C. C. Chirilă and M. Lein, Influence of nuclear vibration on harmonic generation in molecules, *J. Phys. B* **39**, S437 (2006).
- [62] D. B. Milošević, W. Becker, and R. Kopold, Generation of circularly polarized high-order harmonics by two-color coplanar field mixing, *Phys. Rev. A* **61**, 063403 (2000).
- [63] C. C. Chirilă and M. Lein, Strong-field approximation for harmonic generation in diatomic molecules, *Phys. Rev. A* **73**, 023410 (2006).
- [64] F. Mauger, A. D. Bandrauk, and T. Uzer, Circularly polarized molecular high harmonic generation using a bicircular laser, *J. Phys. B* **49**, 10LT01 (2016).
- [65] P. Antoine, B. Piraux, and A. Maquet, Time profile of harmonics generated by a single atom in a strong electromagnetic field, *Phys. Rev. A* **51**, R1750 (1995).
- [66] C. Chandre, S. Wiggins, and T. Uzer, Time-frequency analysis of chaotic systems, *Physica D (Amsterdam)* **181**, 171 (2003).